Water Science & Technology

Influence and mechanism of solids on the air pressure fluctuations on the building drainage system

Ping Xu ✉*, Ke Wang, Xue Fu, Zhuangzhuang Liu and Yilin Song

Key Laboratory of Urban Stormwater System and Water Environment, Ministry of Education, Beijing University of Civil Engineering and Architecture, Beijing 100044, China
*Corresponding author. E-mail: xuping@bucea.edu.cn

PX, 0000-0002-5885-5955

ABSTRACT

The conventional building drainage system was constructed based on the theory of two-phase flow involving water and air. However, the drainage system contained a more intricate three-phase flow, encompassing water, air, and solids, which was relatively overlooked in research. This study addressed the impact of solids on pressure fluctuations, air flow rates, and hydraulic jump fullness within the drainage system, considering three factors: the mass factor, cross-section factor, and viscosity. The investigation was conducted within a single-stack system using both experimental methods and CFD simulations. The findings revealed a positive correlation between both positive and negative pressures and above three factors. The mass factor and the cross-section factor had a more significant impact on the negative pressure of the system. The maximum growth rates of negative pressure extremes under different mass and cross-section factors reached 7.72 and 16.52%, respectively. In contrast, the viscosity of fecal sludge had a slightly higher effect on the positive pressure fluctuation of the drainage system, with the maximum growth rate of positive pressure extremes at 3.41%.

Key words: air pressure, cross-section factor, mass factor, solid, viscosity

HIGHLIGHTS

- Mass factor and cross-section factor are positively correlated with air pressure.
- Viscosity has a slightly greater effect on positive pressure.
- The negative pressure is proportional to the air flow rate discharging solids.
- Hydraulic jump fullness is the main reason for the variation of positive pressure.

GRAPHICAL ABSTRACT
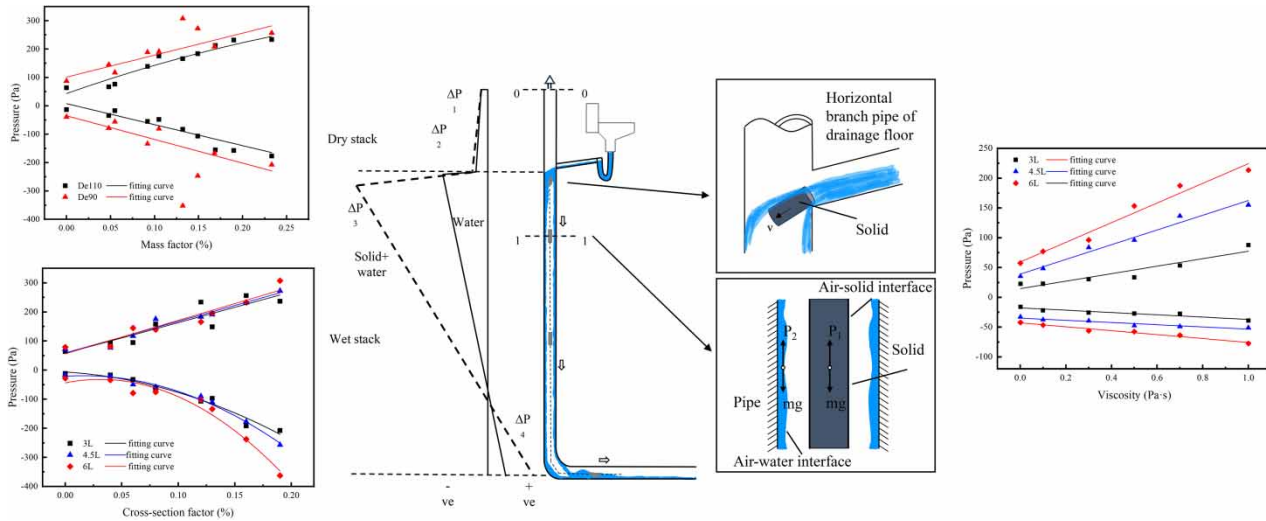
1. INTRODUCTION

The fundamental requirement of a building drainage and vent system is that it carries away any appliance discharge while at the same time preventing any foul odor ingress into the habitable space from the drainage network (Swaffield *et al.* 2004). The lack of water resources is an issue that is common to some global threats (Foster & Ait-Kadi 2012), with urban population growth, accelerated urbanization (Gao *et al.* 2014), and the impact of climate change (Arnell *et al.* 2011; Miranda *et al.* 2011). In this context, using water-saving sanitary wares becomes widespread in many countries (Dolnicar *et al.* 2012; Du *et al.* 2021), which increases the percentage of gross solids in sewers (McDougall & Swaffield 2000). Previous investigations generally overlooked solids in building drainage systems, opting for a simplified analysis that reduced the three-phase flow of water, air, and solid (Cheng *et al.* 2008; Baroni *et al.* 2018) to a two-phase flow model of water and air (Gormley *et al.* 2021). Consequently, it became imperative to investigate the impact of solids on air pressure fluctuations within drainage systems to enhance the optimization of design and operation aspects.

In the investigation of air pressure fluctuations in building drainage systems, numerous researchers approached the subject from a two-phase flow perspective, thereby formulating a theoretical framework for building drainage systems. The water film flow theory proposed by American scholars (Wyly 1952; Wyly *et al.* 1979) was widely adopted by many countries and served as a fundamental theory for the design of building drainage systems. Following this, Lillywhite *et al.* (1969) derived an equation that established the correlation between air flow rate and drainage discharge rate within the vertical stack. This equation was based on the pressure reduction resulting from the drainage of the cross-branch. A research institute in India also confirmed that the value of negative pressure changes (h) induced by the negative pressure-sucking effect is a function of the terminal velocity (v_t), expressed as $h = f(v_t, Q/D)$. Certain scholars delved into refining pressure change parameters and terminal flow rate equations by examining variations in pipe materials (Zhang 2022) and ventilation methods (Guan 2022). In the investigation of solids in building drainage systems, the predominant focus lied on their transportation performance within horizontal drain pipes. Specifically, researchers aimed to understand how altering pipe slope, diameter, and drainage volume impacted the smooth discharge of solids in horizontal pipes (McDougall & Swaffield 2003; DeMarco *et al.* 2013; Campbell 2017). However, when it came to the influence of solids on air pressure fluctuations, only a limited number of scholars have conducted exploratory studies. For instance, Gormley (2007) conducted experiments involving the discharge of $250 \times 65 \times 10$ mm maternity pad in 16 layers through DN150 drainage vertical stack, and observed a pressure surge in branch-to-stack junction due to the solids. Another study by Zhang (2018) involved the discharge of 80 mm $\times$ 25 mm solid gelatinous cotton simulants in a specialized single vertical stack drainage system. The results indicated that the addition of solids led to an increase in pressure extremes, though the increase was not deemed significant. Thus, while it was evident that the addition of solids did impact air pressure fluctuations within the drainage system, the specific mechanisms of this influence warrant a more in-depth exploration. This study employed enteric-coated simulant materials and fecal

sludge simulants, utilizing both the experimental approach of instantaneous flow discharge from a flush toilet and Computational Fluid Dynamics (CFD) simulations. The investigation aims to explore the effects of mass factor, cross-section factor, and viscosity on pressure extremes, air flow rate, and hydraulic jump fullness within the drainage system. The objective is to elucidate the reasons and mechanisms behind the influence of solid on air pressure fluctuations in the drainage system, considering three dimensions.

2. MATERIALS AND METHOD

2.1. Introduction of the experiment

A full-scale experimental setup was implemented to investigate the impact of solids' mass and volume size on air pressure fluctuations. Subsequent to the full-scale drainage test and taking operability into account, a 2D model was created using the commercial software ANSYS Fluent. The study also involved the examination of the effect of viscous coefficients through the CFD simulation approach.

2.2. Experimental system

In this study, a four-story (12.6 m) full-scale single-stack drainage system was constructed, as depicted in Figure 1.

The test drainage pipe was constructed from polymethyl methacrylate (Plexiglas). The connecting fittings for the toilet and tee were made of rigid polyvinyl chloride (PVC-U). The pipe diameters used were De110 or De90. The horizontal drain pipe at each level was 0.7 m in length, connecting to the vertical stack through a 90° water tee. The bottom of the vertical stack was linked to the 22 m horizontal drain pipe with a 90° elbow. A jet siphon toilet and a constant flow drainage device were installed on the third and fourth floors horizontal branch pipe. Pressure sensors (GE DruckPTX 610, measurement range of ± 1 kPa, an accuracy of $\pm 0.5\%$ and acquisition cycle of 200 ms) were installed in the drainage riser, horizontal branch pipe and horizontal main drain. The air tightness of the drainage system is intact, and there is no leakage.

A self-designed control system for the drainage system test comprises a PLC automation control cabinet, an electromagnetic automatic feeding, drainage system, and a PC. The PLC control cabinet and the PC device are shown in Supplementary material, Figure S1.

The flush volume of the toilet was regulated through a liquid level sensor in the tank. To minimize manual pressing time errors on the drainage valve, an electromagnetic valve was used for automatic drainage, with a response time of 2 s. For each test, solid was manually placed into the toilet bowl. Throughout the testing process, the data acquisition system collected data
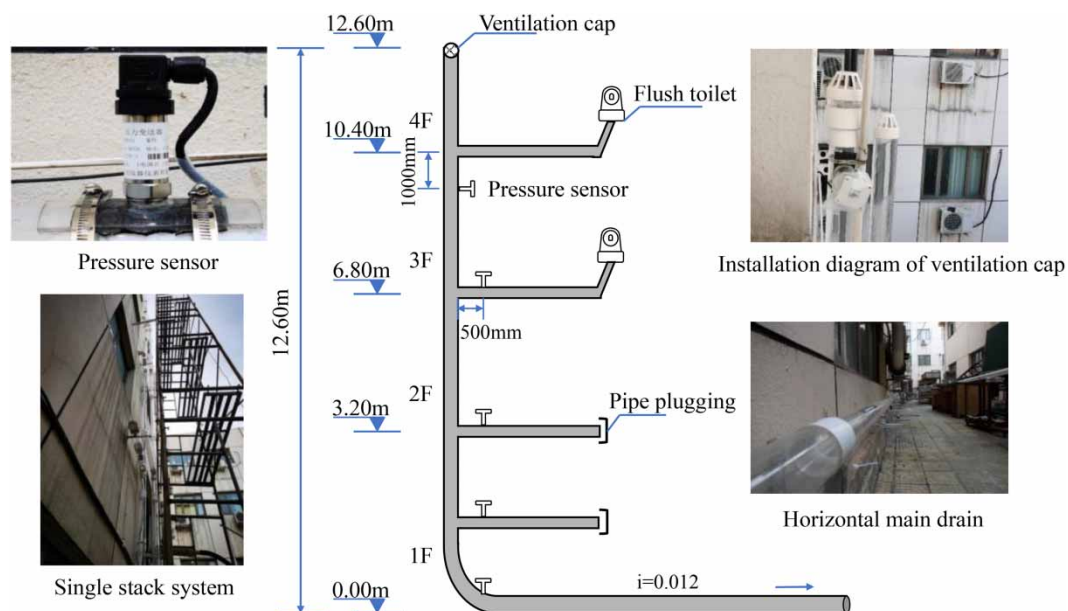
Figure 1 | Full-scale single-stack drainage testing facilities.

from pressure sensors at a sampling frequency of 200 ms, over a duration of 40 s. After completion of data collection, the data were exported to a computer for further analysis and calculations.

2.3. Materials

Solids in drains constituted a complex composition. Friedler *et al.* (2008) found sewer fouling includes feces, toilet paper, tampons, wet wipes, etc. Lewis & Heaton (1997) classified feces into seven types, from hard lumps to pastes, representing common human fecal shapes. In this study, enteric-coated solid and fecal sludge simulants were used to investigate the effect of solid and fluid on air pressure fluctuations in drainage systems.

2.3.1. Enteric-coated solids

Referring to the solids used in the flush performance test for toilets as specified in Appendix E of *Sanitary Wares* (General Administration of Quality Supervision 2015), a mixture of 75 g of water and 22 g of soil was prepared and placed into a bowel stimulant. The simulant was then wrapped with gauze. Each solid had a mass of approximately 100 g, a length of around 200 mm, and a diameter of about 20 mm. 200 g of solids were discharged from two enteric-coated simulants, and so on.

2.3.2. Fecal sludge

The study of Radford *et al.* (2015) determined that the formulation consisted of kaolin, topsoil, water stirred with a viscosity of 0.7 Pa·s, and a density of about 1.165 g/cm^3.

2.4. Test methods and parameters

2.4.1. Mass factor

The mass factor, denoted as the ratio of solid mass to the sum of solid and liquid mass, was defined to characterize the influence of solid mass on flow rate and air pressure fluctuations in the drain. It was calculated using the following Equation (1):

$$\alpha = \frac{M_s}{M_s + M_l} \tag{1}$$

where α is the mass factor; M_s is the solid mass, g; M_l is the liquid mass corresponding to the maximum instantaneous drainage flow rate, g.

In this study, an instantaneous drainage flow test was conducted to determine the instantaneous drainage flow rate of the WC at various discharge volumes. The mean values of the maximum instantaneous flow rates for discharge volumes of 3, 4.5, and 6 L at a vertical stack diameter of De110 were found to be 1.0, 1.70, and 2.00 L/s, respectively. Similarly, the mean values for discharge volumes of 3, 4.5, and 6 L at a vertical stack diameter of De90 were 1.03, 1.77, and 2.02 L/s. The corresponding masses for the aforementioned instantaneous drainage volumes were calculated based on the density of water as 1 g/cm^3.

The test conditions, specified in terms of the mass factor, are presented in Table 1.

2.4.2. Cross-section factor

The cross-section factor was used to characterize the influence of solid cross-sectional dimensions on air pressure fluctuations in the stack. It was calculated as shown in Equation (2):

$$\gamma = \frac{C_s}{C_p} \tag{2}$$

Table 1 | Mass factor test program

Mass factor	0.00	0.05	0.06	0.09	0.11	0.13	0.15	0.16	0.17	0.19	0.23
Solid (g)	0	100	100	100	200	300	300	200	400	400	300
Solid and liquid (g)	–	2,100	1,800	1,100	1,900	2,300	2,000	1,200	2,400	2,100	1,300

where γ is the cross-section factor; C_s is the cross-section area of solid, m²; C_p is the cross-section area of stack, m². Specific test conditions are shown in Table 2.

2.4.3. Viscosity

To delve deeper into the impact of the fluidized state of fecal sludge on air pressure fluctuations in the drainage system, CFD was used to simulate the discharge of fecal sludge with different viscosity μ. The construction details of the CFD model are provided in Section 3.

The simulated density conditions of fecal sludge, based on findings from literature research (Penn *et al.* 2018; Mupinga *et al.* 2020), are presented in Table 3.

2.4.4. Test method for hydraulic jump fullness

Hydraulic jump fullness is numerically equal to the ratio of water level height to pipe diameter.

The water level height was measured using the following method: a range of 0–60 cm at the first end of the horizontal drain pipe was selected as the observation range for hydraulic jump height and fullness, as illustrated in Supplementary material, Figure S2. A vertically oriented steel ruler was positioned at 10 cm intervals, with a total of 7 measurement points established along the horizontal drain pipe. During the test, a high-speed video camera recorded the hydraulic jump change process. Subsequently, the video was imported into the computer; the frames were played to capture the water level height data using Kinovea software.

3. CFD MODEL ESTABLISHMENT

3.1. Geometrical model and meshing

A four-story drainage system, 12 m in height, with a De110 pipe diameter, was constructed in equal scale using ANSYS-ICEM software. To eliminate the influence of water and airflow in the branch pipes of other floors on the calculation results, only the drainage conditions of a single floor were considered. The horizontal branch pipe and vertical stack were interconnected through a 90° smooth water tee, and double 45° elbows connected the vertical stack and the horizontal drain pipe. The mesh division of the articulation part is illustrated in Supplementary material, Figure S3.

3.2. Calculation method and control conditions

The flow of fecal sludge in the pipe was modeled using the following continuity and momentum equations:

$$\frac{\partial}{\partial t}\iiint_V \rho \, dx dy dz + \iint_A \rho \vec{v} \cdot n dA \tag{3}$$

$$\rho \frac{d\vec{V}}{dt} = \rho \vec{F} + \frac{\partial \vec{P}_x}{\partial x} + \frac{\partial \vec{P}_y}{\partial y} + \frac{\partial \vec{P}_z}{\partial z} \tag{4}$$

where V is the control body; A is the control surface; ρ is the fluid density, kg/m³; v is the fluid velocity, m/s; and t is the

Table 2 | Cross-section factor test program

Cross-section factor	0.04	0.06	0.08	0.12	0.13	0.16	0.19
Stack cross-sectional area (10^{-3} m²)	7.85	5.02	7.85	7.85	5.02	7.85	5.02
Solid cross-sectional area (10^{-3} m²)	0.31	0.31	0.63	0.94	0.63	1.26	0.94

Table 3 | Viscosity test program

Viscosity (Pa·s)	0.00103	0.1	0.3	0.5	0.7	1.0
Density (g/cm³)	1,350					
Discharge volume (L)	3, 4.5, 6					

computational time, s. F is the mass force on the bit mass of the fluid; P_x, P_y, and P_z are the components of the internal stress tensor of the fluid in the three directions; and $\rho(d\vec{V}/dt)$ is the combined force exerted on the fluid mass per unit volume.

ANSYS Fluent provided three multiphase flow models: the volume of fluid model (VOF), the mixture model, and the Eulerian model. In the working condition simulated in this test, the boundary between the liquid phase and the gas phase was more pronounced. Water flowed into the vertical stack from the cross-branch, carrying the upper air down and compressing the lower air close to the piston flow. Therefore, the VOF model was used in this study.

Referring to examples from previous studies on air flow rate in drains (Zhang *et al.* 2022; Guo *et al.* 2023), the realizable k-epsilon turbulence model was selected. This model exhibits better phase characteristics than curved, rotating, and swirling streamlines. Fluent predominantly utilized the Finite Volume Method (FVM) as the main discretization format, with the Pressure Implicit Split by Operator (PISO) algorithm specifically chosen for non-constant flows and severe mesh shape variations. The volume fraction was discretized using the QUICK format to visualize the two-phase interface. The first-order upwind format was employed, for the discretization of momentum, turbulent pulsation kinetic energy, and volume fraction.

In the boundary condition setup, the drainage cross-branch was designated as the velocity inlet, with the turbulence intensity maintained at a constant value. The horizontal main outlets at the top and bottom of the exhaust pipe were connected to the atmosphere and were configured as pressure outlets. The surface pressure was set to 0 Pa, and the direction was perpendicular to the boundary. The turbulence intensity and hydraulic diameter of the outlets were both set to 3% and 100 mm, respectively.

Given that the drainage system was initially filled with air, the water content (phase-1) of the entire system was initialized to 0. The gas-phase viscosity was set to 1.7894×10^{-5} kg/(m·s) during the initialization of the convection field.

Following initialization, a time step of 0.02 s was chosen considering the estimated flow rate and the Courant number. The Courant number was calculated by dividing the distance traveled by the fluid within a time step by the unit length of the rectangular grid. The simulation was conducted over 1,000 time-steps, and the grid size was adjusted to ensure compliance with the stability criterion.

3.3. Model validation

In order to validate the numerical methods employed in the CFD model for simulating pressure and flow rate, the CFD simulation results were compared with the measured outcomes to verify their accuracy.

The pressure variation for discharging fecal sludge with a viscosity of 0.7 Pa·s on one-story is given in Supplementary material, Figure S4.

As shown in Supplementary material, Figure S4, the maximum pressure of the simulation results and the measured results are generated at 4 s, and the pressure fluctuation time is concentrated in 2–6 s. In the actual test, the transverse branch pipe on the non-drainage floor hindered the water flow during the descending process, resulting in a reduced descent speed and smaller pressure fluctuations. In the simulation process, the cross-branch pipe of the non-drainage floor was modeled as a smooth pipe wall, leading to more pronounced simulation results compared to the actual test. Nevertheless, there was satisfactory agreement between the predicted and measured data from the CFD model. This suggests that the algorithm used in the CFD model accurately predicted the air velocity and pressure changes in the drainage system discharging fecal sludge.

4. RESULTS AND DISCUSSION

4.1. Influence of the mass factor

4.1.1. Pressure extreme

As the mass factor increases, the variation of the system pressure extremes is shown in Figure 2.

From Figure 2, it is evident that with the increase of the mass factor, the absolute values of the positive and negative pressure extremes of the system exhibit an upward trend. Specifically, for the case of mass factor 0 at De110 pipe diameter, the positive and negative pressure extremes are 71 and -17 Pa, respectively, with growth rates of 2.30 and 7.72% in the presence of solids. When the mass factor reaches its maximum value of 0.23, the system's positive and negative pressure extremes reach 233.87 and -176.80 Pa, respectively. In comparison to the De110 pipe diameter, the positive and negative pressure increase of the system under the De90 pipe diameter is more substantial, with growth rates of 1.94 and 4.34%. The positive and negative pressure extremes of the system reach as high as 307.49 and -352.24 Pa, respectively.

Tanabe *et al.* (2013) demonstrated that the more solid waste was discharged, the more drastic the negative pressure fluctuation was during instantaneous flow drainage from a toilet with a 6-L flow rate, which aligns with the findings of this study.
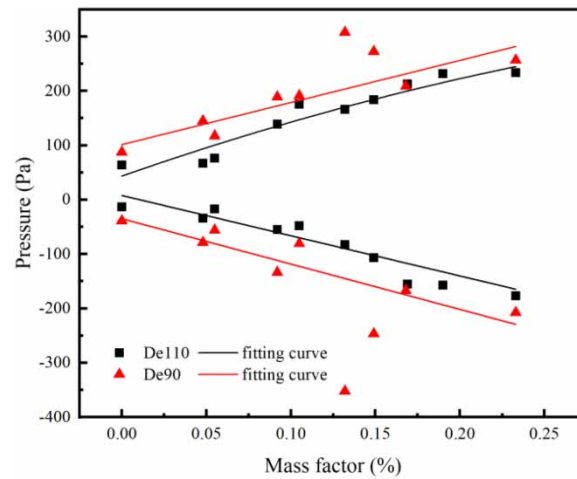
Figure 2 | Extreme pressure of the system with different mass factors.

Moreover, as observed in Figure 7, when the pipe diameter decreases, the system pressure extremes undergo more drastic changes. Guan *et al.* (2020) studied that increasing the diameter of the vent pipe can enhance the drainage system's capacity, resulting in more stable positive and negative pressure fluctuations, which is consistent with the outcomes of this study. As depicted in Figure 6, when the pipe diameter is De110, the system's positive and negative pressure changes remain more stable with the increase of the mass factor. Conversely, the system's positive and negative pressure fluctuate more at mass factors of 0.13 and 0.15, indicating that as the pipe diameter decreases, the ventilation cross-section in the pipeline diminishes, leading to an increase in turbulence in the three-phase flow within the vertical stack. During such conditions, the system's pressure changes are influenced by the impact of the cross-section factor, which will be further discussed in Section 4.2.

4.1.2. Air flow rate

To further illustrate the effect of the mass factor on the drainage system, the variations in ventilation flow rate corresponding to different mass factors were determined for the De110 pipe diameter drainage system under the four-story drainage condition. The results are shown in Figure 3.
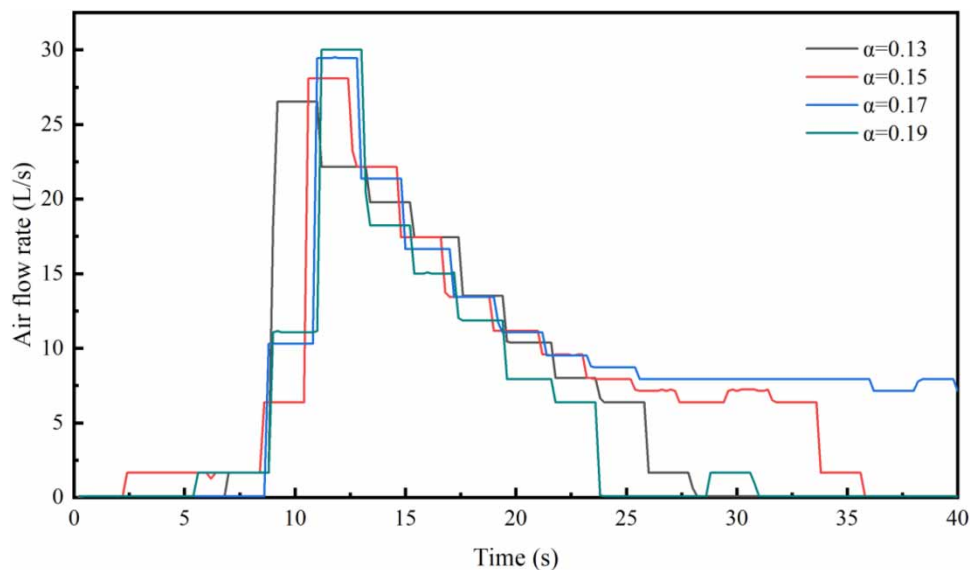
Figure 3 | Air flow rate variation under different mass factors.

As shown in Figure 3, with the increase of mass factor, the maximum value of the system ventilation flow rate increases, and the time of the peak value appearance is delayed. Compared with the 0.13 condition, the extreme value of the ventilation flow rate under the 0.15, 0.17, and 0.19 conditions increase by 5.92, 11.01, and 13.16%, respectively. The time of appearance of the extreme value is delayed by 1.4, 1.8, and 2 s. Since the ventilation flow rate is related to the change of the negative pressure, the pressure fluctuation at the minimum pressure floor is shown in Figure 4.

As shown in Figure 4, as the mass factor increases, the minimum pressure increases. The appearance of negative pressure extremes is delayed, and the time experienced for pressure fluctuations decreases to 3.9, 3.4, 2.6, and 2.4 s, respectively.

Wise and Swaffield (Wise & Swaffield 2012) showed the relationship between air flow rate and drainage flow in a vertical drain stack as shown in Equation (5):

$$Q_a = K\left(\frac{\pi D^2}{4}v_t - Q_w\right) \tag{5}$$

where K is the empirical coefficient, which is taken as 1.5 in the extended roof ventilation system; D is the diameter of vertical stack, cm; Q_w is the drainage flow rate, cm^3/s; Q_a is the air flow rate, cm^3/s; v_t is the terminal flow rate, m/s.

According to Equation (5), the terminal flow rate was one of the main factors affecting the air flow rate. Whereas the mass of solids was different, its falling speed in the vertical stack drain was different and eventually affected the terminal flow rate. To calculate the falling velocity of solids, based on the results of the study presented in Figure 8, the pressure transient time was considered as the time it takes for solids to fall to the horizontal drain pipe from the height of the drainage floor (10.4 m). The velocities of the solid falling process, with an increase in the solid–liquid mass ratio, were calculated to be 2.67, 3.06, 4.00, and 4.33 m/s, respectively. Comparing with Figure 3, it can be observed that with the increase of the mass factor, the negative pressure extreme of the system increases. This is consistent with the trend of solid velocity, i.e., as the solid velocity increase, the terminal flow rate also increased due to the shear force at the air–solid interface and the air–water interface, leading to an increase in the ventilation flow rate.

After solids were added to the vertical stack, a specific moment was reached where solid, water gravity, and air friction attained equilibrium. At this point, gravitational acceleration was zero, and the water flow velocity reached its extreme value, approximately equal to the air velocity – representing the traditional two-phase flow terminal velocity. During this phase, the system reached its minimum pressure. In the falling process of solids, air–solid and air–water interfaces were formed as the velocity of the solid increased. These formations were caused by the influence of shear force, resulting in an
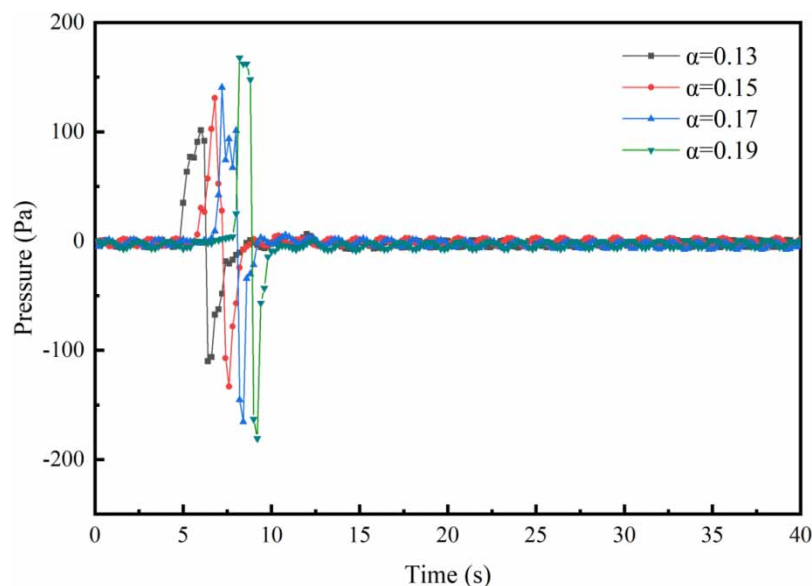
Figure 4 | Variation of pressure at the minimum pressure floor for different mass factors.

increase in the terminal flow rate. Therefore, with an increase in the mass factor, the ventilation flow rate of the drainage system also increased.

4.1.3. Hydraulic jump fullness

Measured at different mass factors in the De110 pipe diameter, within the starting section of the horizontal drain pipe's 60 cm length, the change in hydraulic jump fullness was examined to explore the positive pressure change rule in the drainage system. The results are shown in Figure 5.

As shown in Figure 5, the peak of hydraulic jump fullness in the horizontal drain pipe is higher with the increase of the mass factor, and the peak of the hydraulic jump occurs in the range of 15–20 cm from the vertical stack. Then the water flow becomes gradually gentle after 40 cm at the beginning of the horizontal drain pipe. The fullness of hydraulic jump reduces to 30% even less, which is negatively correlated with the mass factor. When the mass factor increases from 0.13 to 0.15, 0.17, and 0.19, the peak hydraulic jump fullness increases by 1.23, 4.94, and 12.35%, respectively. Positive pressure extremes within the drainage system are generally generated at the bottom of the vertical stack at the beginning of the horizontal drain pipe. The positive pressure extremes are correlated with the hydraulic jump, therefore the positive pressure fluctuations at the floor of the maximum positive pressure value were determined, as shown in Figure 6.

As can be seen from Figure 6, with the increase in the mass factor, the positive pressure extremes of the maximum positive pressure floor increase, the time of the extreme value is delayed, and the pressure fluctuation time is concentrated in 5–10 s.

The hydraulic jump is caused by a sharp change in the flow pattern of the water at the beginning of the horizontal drain pipe. This change affects both the height and the fullness of the hydraulic jump in the stack. Consequently, it hinders the airflow in the horizontal drain pipe, resulting in a steep increase in positive pressure (Najafzadeh 2019). From Figures 9 and 10, it can be observed that the hydraulic jump fullness, after adding solids to the drainage system, is directly proportional to the trend of the positive pressure of the system. In other words, with the increase of the mass factor, the potential energy of the solids in the drainage system is converted into kinetic energy, intensifying the hydraulic jump fluctuation in the horizontal drain pipe. Consequently, this leads to more significant changes in positive pressure.
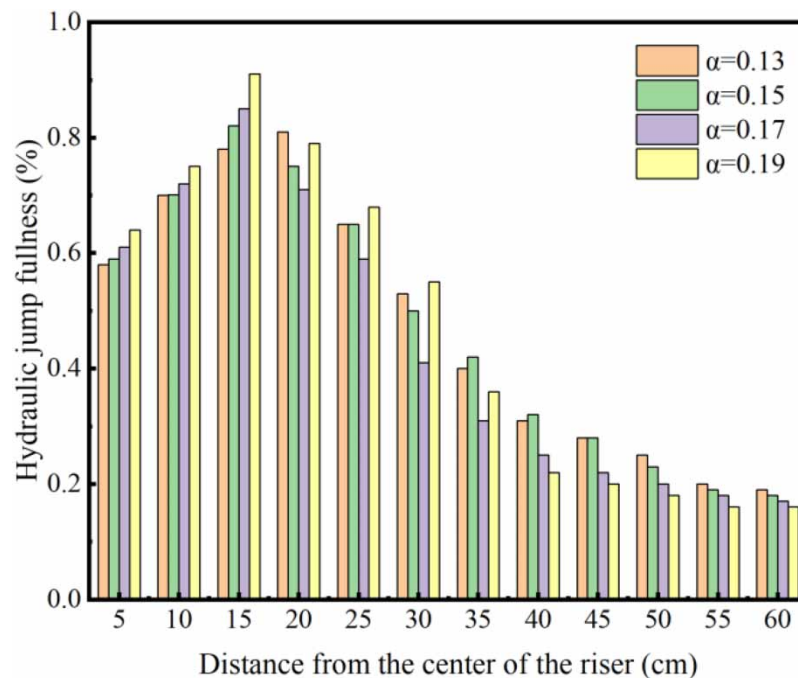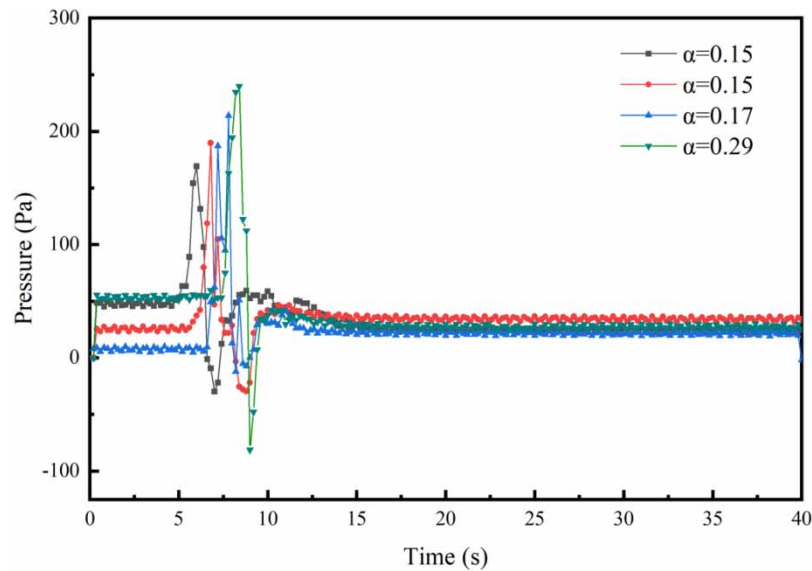

Figure 5 | Hydraulic jump fullness in horizontal drain pipes with different mass factors.

Figure 6 | Variation of pressure at the maximum positive pressure floor.

4.2. Influence of the cross-section factor

4.2.1. Pressure extreme

The variation of the system pressure extremes with the increase of the cross-section factor is shown in Figure 7.

From Figure 7, it is evident that with the increase of the cross-section factor, both the positive and negative pressure extremes of the system show noticeable increasing trends. Additionally, the negative pressure extremes change more drastically than the positive pressure extremes. When the cross-section factor is 0, the positive pressure extreme value of the system ranges from 66.78 to 92.51 Pa. However, when the cross-section factor reaches its maximum value of 0.19, the positive pressure extreme value increases in the range of 236.54–307.49 Pa. The growth rate for water volumes of 3, 4.5, and 6 L is 2.69, 2.76, and 2.88%, respectively. The degree of change in negative pressure extremes is more significant compared to
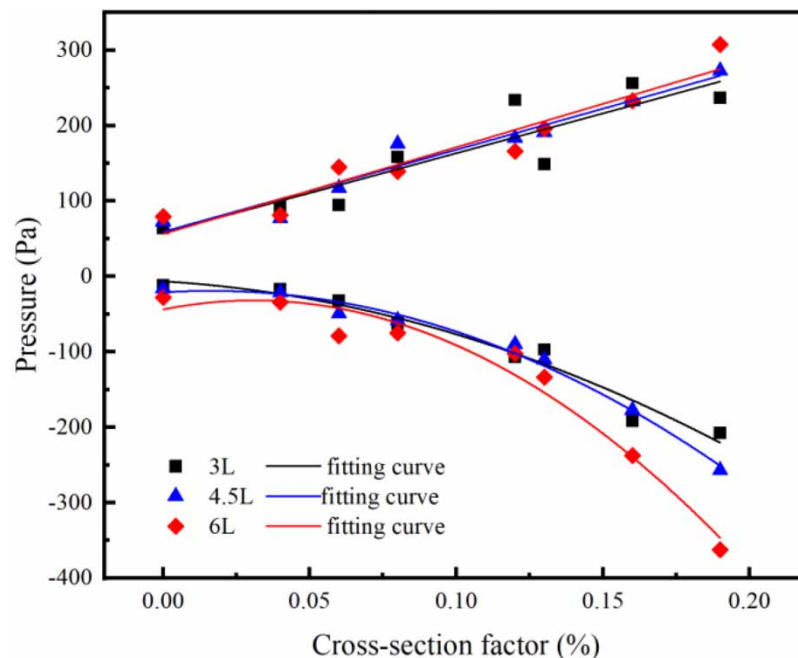
Figure 7 | Variation of positive and negative system pressure extremes with a cross-section factor.

positive pressure. The negative pressure extremes of the system increase from 16.73, 17.27, and 33.96 Pa to 207.56, 256.99, and 362.24 Pa, with growth rates of 16.52, 16.06, and 11.92%, respectively, under the three drainage volumes.

According to Wyly & Eaton (1961) and Swaffield & Campbell (1995), the negative pressure suction and the hydraulic jump at the bottom of the vertical stack increased with the increase of the drainage flow rate. This phenomenon led to an increase in both positive and negative pressure extremes of the system, which is consistent with the results of this study.

When solids were added to the system, an increase in the cross-section factor intensified the impact of solids on the air path of the water curtain at the branch-to-stack junction. Consequently, there was a greater loss in the water curtain caused by solids. In the vertical stack, the proportion of solids in the pipe section increased, leading to more turbulent air flow in the vertical stack. This increased turbulence amplified the friction between the air–solid and the air–water interface, resulting in a significant rise in loss along the path. Therefore, the negative pressure change became more prominent. The positive pressure extreme value of the drainage system typically occurred at the bottom of the stack. When solids, along with water, descended from the stack to the horizontal pipe, congestion occurred at the beginning of the horizontal pipe. The greater the proportion of solids in the pipe cross-section, the more pronounced the blockage of airflow in the horizontal drain pipe. This phenomenon led to an increased positive pressure extreme value of the system.

4.2.2. Air flow rate

Since the variation in negative pressure was more pronounced at 6 L of discharge volume, the variation of air flow rate with cross-section factor at 6 L of discharge volume was determined and is shown in Figure 8.

As seen in Figure 8, the maximum value of the system air flow rate increases with the increase of the cross-section factor, and the overall change in the air flow rate is consistent with the observations from the previous section, exhibiting the phenomenon of delayed extreme values. When the cross-section percentage is 0.13, 0.16, 0.19, compared with the 0.08 condition, the extreme value of the air flow rate increases by 9.32, 14.50, 18.41%, and the time of the extreme value is delayed by 0.2, 0.4, 2.6 s, respectively. Meanwhile, the determination of the pressure changes on the minimum pressure floor with different cross-section factors under the water volume of 6 L is shown in Figure 9.

As can be seen in Figure 9, with the increase of the cross-section factor, the negative pressure extremes of the minimum pressure floor increase. The minimum pressure appeared with delay time, which occurred at 5.8, 7.2, 7.8, and 8.2 s, and the pressure fluctuations were between 4 and 12 s, which is consistent with the results of the variation of air flow rate.

According to the equation proposed by Wise & Swaffield (2012), the negative pressure extremes were proportional to the air flow rate when the system was drained only. In conjunction with the results of subsection 4.1.2, the same holds in the case
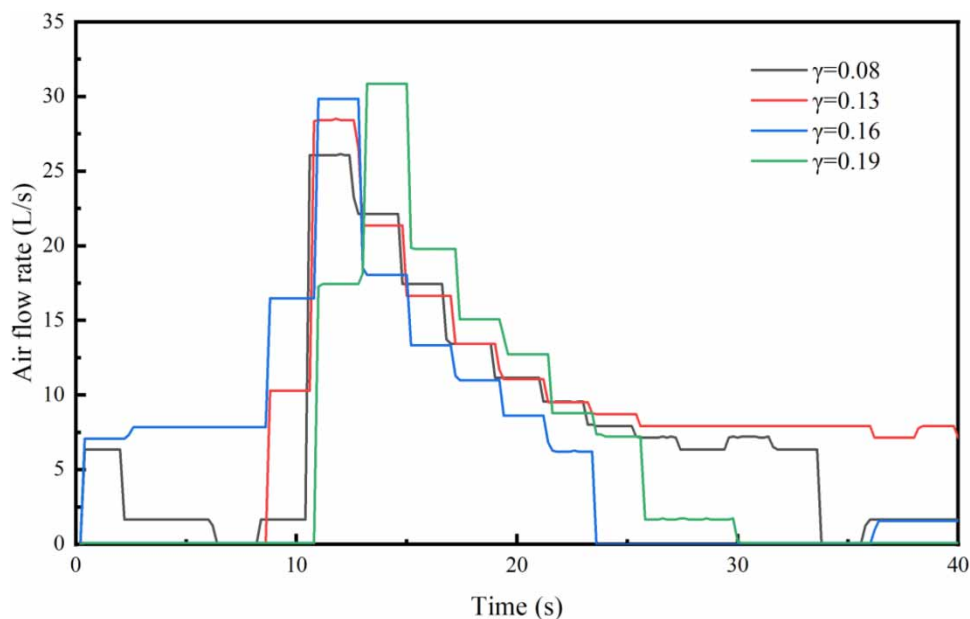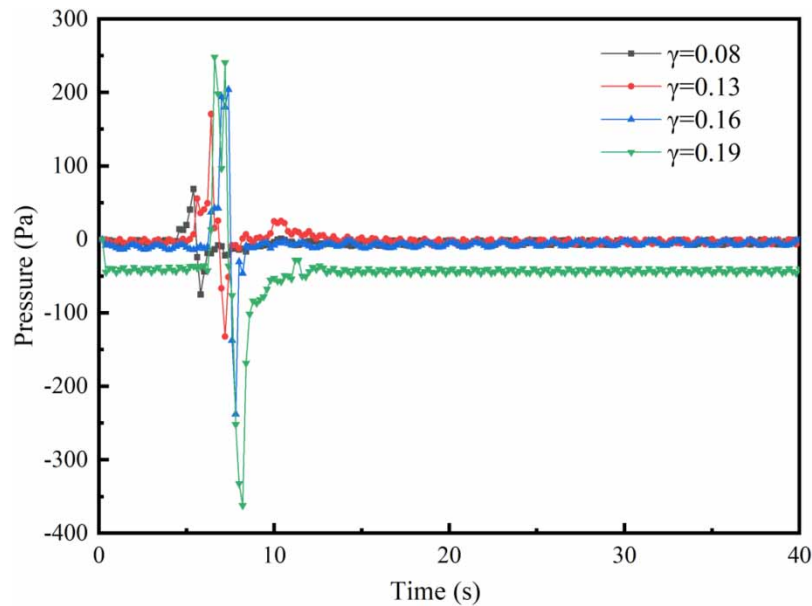

**Figure 8** | Air flow rate with a cross-section factor under 6 L of water volume.

Figure 9 | Variation of pressure at the minimum pressure floor for different cross-section factors.

of discharged solids. However, comparing the results of subsection 4.1.2, it was found that with the increase of cross-section factor, the change of both air flow rate and negative pressure was more significant than the change of mass factor. It is inferred that when the volume of solids increases to a critical value, the cross-section factor of solids determines the evolution of the air flow rate and negative pressure in the drainage system better than the mass factor. Due to the three-phase motion of air, water, and solid in the pipeline, the friction between the air–solid interface and the air–water interface increased dramatically, resulting in a larger pressure drop.

4.2.3. Hydraulic jump fullness

The variation of hydraulic jump fullness at the beginning 60 cm of the horizontal pipe for different cross-section factors at 6 L discharge volume is shown in Figure 10.

As shown in Figure 10, the peak value of hydraulic jump fullness in the horizontal drain pipe increases with the increase of the cross-section factor. The peak value of hydraulic jump occurs in the range of 10–20 cm from the vertical stack pipe, and
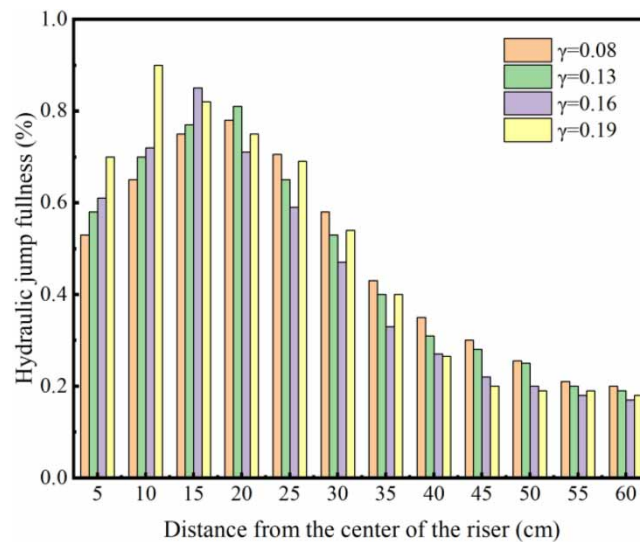
Figure 10 | Hydraulic jump fullness in horizontal drain pipes with different cross-section factors.

the hydraulic jump fullness is basically lower than 30% after a distance of 40 cm from the beginning of the horizontal stack pipe. The peak hydraulic jump fullness is 78% when the cross-section factor was 0.08 and increases to 81, 85, and 90% when the cross-section factor increased to 0.13, 0.16, and 0.19, respectively. The variation of positive pressure fluctuation with cross-section factor for the floor with maximum positive pressure value is shown in Figure 11.

From Figure 11, it can be seen that with the increase of the cross-section factor, the positive pressure extreme value of the maximum positive pressure floor increases, the extreme value appears earlier, and the pressure fluctuation time is in the range of 5–15 s.

From Figures 10 and 11, it can be seen that as the cross-section factor increases, the hydraulic jump fullness increases. The result is the same as the trend of the hydraulic jump and the positive pressure extremum in subsection 4.1.3. The results of the previous research of our group (Xu et al. 2023) also showed that the hydraulic jump fullness was the leading cause of the positive pressure change in the horizontal drain pipe, which was directly proportional to the discharge volume and inversely proportional to the pipe diameter, which is consistent with the results of this test.

Upon comparing the preceding findings, it becomes evident that the variation in hydraulic jump fullness exhibits a more consistent pattern in response to the mass factor. Conversely, an augmentation in the cross-sectional factor was observed to induce an elevation in the peak hydraulic jump fullness, concomitant with a forward shift in its position. This phenomenon may be attributed to the influence of solids on altering the flow characteristics. According to Li et al. (2015), if the flow rate of sand transport water in the steep slope was specific, the greater the intensity of Gaza upstream was, the closer it was to the upstream of the beginning of siltation. When the intensity of Gaza was unchanged, the smaller the flow rate was, the closer it was to the upstream of the start of siltation, which was consistent with the present experimental results.

4.3. Influence of the viscosity

The variation of pressure extremes of the drainage system with different viscosity is shown in Figure 12.

As shown in Figure 12, the system's positive and negative pressure extremes increase with the increase of fecal sludge viscosity and drainage volume. With the rise in viscosity, the growth rate of positive pressure extremes of the system is 2.89, 3.41, and 2.71% for the water volume of 3, 4.5 and 6 L. The growth rate of negative pressure extremes is 1.46, 0.56, and 0.83%, respectively. The system's maximum positive pressure extreme value in all working conditions is 213.20 Pa. The minimum pressure extreme value is −77.40 Pa. It was seen that with the increase of the viscosity, the change of the positive pressure extreme value of the system was slightly higher than that of the negative pressure extreme value. Akhiyarov et al. (2010) concluded that the high-viscosity oil pressure gradient in the pipeline increases with the increase of viscosity, which was consistent with the simulation results.
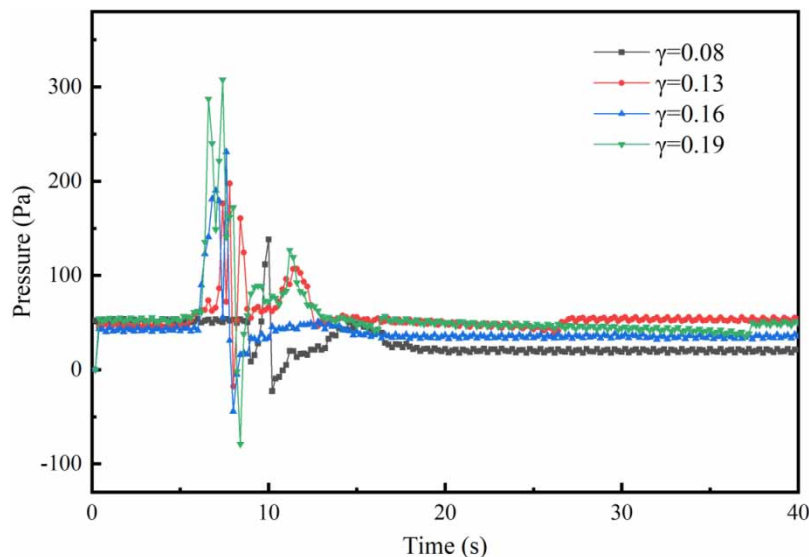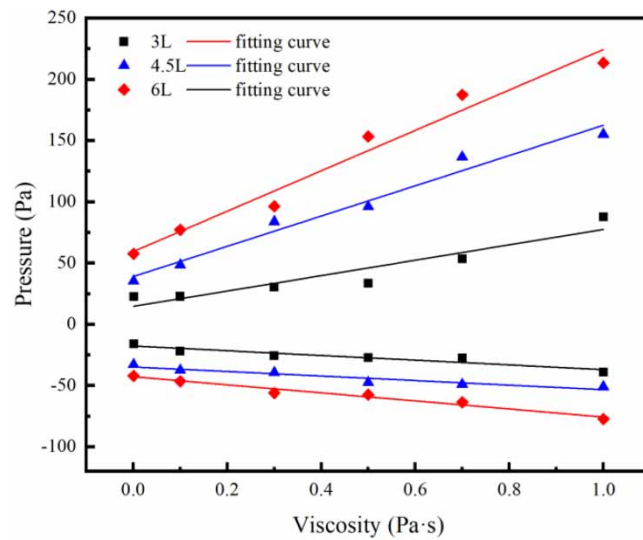

Figure 11 | Variation of pressure at the maximum positive pressure floor.
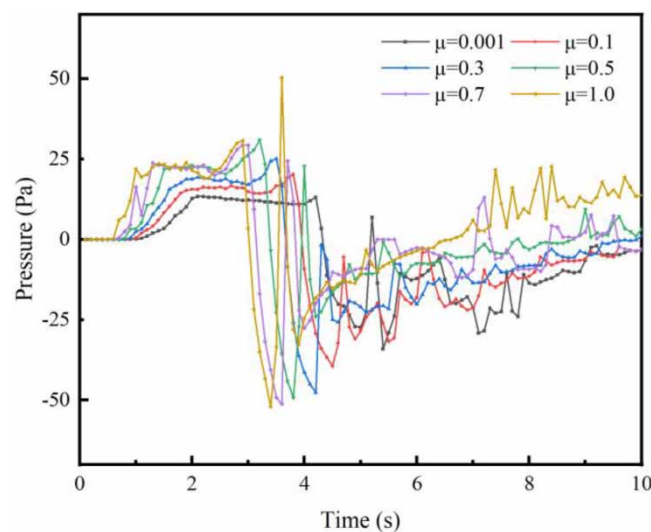
Figure 12 | Variation of pressure extreme value with different viscosities.

The pressure fluctuations at the minimum floor for discharging fecal sludge with different viscosity are shown in Figure 13, and the variation in air flow rate is shown in Supplementary material, Figure S5.

From Figure 13 and Supplementary material, Figure S5, it can be seen that when the viscosity of fecal sludge increases, the negative pressure extreme value and the air flow rate extreme value increase. The time of the extreme value appears earlier, and the system pressure fluctuation is concentrated in 2–8 s. The negative pressure extreme value and the air flow rate extreme value increase when fecal sludge's viscosity grows. With the rise of fecal sludge viscosity, the growth rate of air flow rate poles is 0.11–0.42% compared with the freshwater condition. This is consistent with the previous section's relationship between the air flow rate and negative pressure extremes.

When the drainage system discharged fecal sludge, the friction between the sludge and the airflow was more remarkable as the viscosity increased. When the fecal sludge flows to the junction, the water curtain formed on the airflow resistance was more significant, resulting in greater localized losses. While the sludge fell in the stack, the air in the vertical stack was subject to the shear stress of the sludge falling process, resulting in a more significant pressure drop.

Figure 13 | Variation of pressure at the minimum pressure floor for different viscosities.

The pressure fluctuations at the maximum positive pressure floor for discharging fecal sludge with different viscosity are shown in Figure 14.

From Figure 14, it can be seen that with the increase of fecal sludge viscosity, the positive pressure extremes increase and appear earlier. The pressure fluctuation time is concentrated within 3–6 s.

To facilitate the analysis of positive pressure fluctuations in the horizontal drain pipe, we recorded the change in velocity vector at the beginning of the horizontal drain pipe when discharging freshwater versus fecal sludge, as shown in Supplementary material, Figure S6.

As shown in Supplementary material, Figures S6(a) and S6(b), as the viscosity increases, the hydraulic jump position decreases slightly from the center distance of the vertical stack. Conversely, the hydraulic jump height and the flow rate of fecal sludge increase slightly. With the increase of the discharge volume, it can be seen from Supplementary material, Figures S6(b) and S6(c) that the gradient of fecal sludge flow rate in the drainage pipe increases. Similarly, the hydraulic jump position slightly advances from the center distance of the vertical stack. Wang et al. (1992) found that the mud, due to its higher viscosity, did not have strong turbulence during the hydraulic jump compared to fresh water. Most of the kinetic energy was converted into potential energy during the hydraulic jump of mud, thus increasing the hydraulic jump height. The conclusion was consistent with the study.

For the planar hydraulic jump, Bhagat et al. (2018) investigated that for the hydraulic jump radius
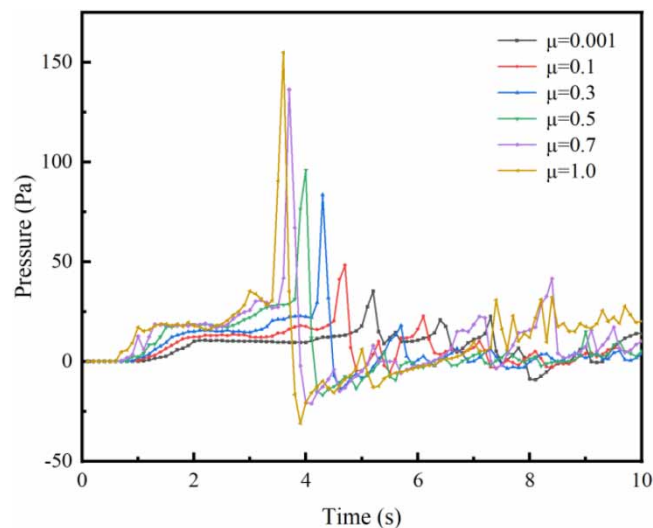
$$\frac{R}{R_0} = \text{constant} \tag{6}$$

where the characteristic length R_0 was given by

$$R_0 = \frac{Q^{3/4}\rho^{1/4}}{\nu^{1/4}\gamma^{1/4}} \tag{7}$$

and

$$\nu = \mu/\rho \tag{8}$$

where R is the radius of hydraulic jump, m; Q is the flow rate, m/s; ρ is the density of the liquid, kg/m^3; ν is the kinematic viscosity of the fluid, m^2/s; γ is the surface tension, mN/m; μ is the viscosity, Pa·s.

Figure 14 | Variation of pressure at the maximum positive pressure floor.

In this study, fecal sludge's density and surface tension were constant, and the CFD simulation was set to change only the kinetic viscosity μ. The hydraulic jump radius was regarded as the distance from the center of the vertical stack pipe to the hydraulic jump position. Hence, the hydraulic jump distance from the center of the vertical stack pipe was positively correlated to the discharge volume Q, and negatively related to the viscosity μ, which agrees with the experimental results.

As the viscosity of fecal sludge increased, the height of the hydraulic jump and the flow rate increased. According to the equation of conservation of energy, a hydraulic jump led to an increase in localized energy loss, which resulted in a sudden rise in air pressure in the drainage system. Therefore, the viscosity was positively correlated with the air pressure fluctuation in the drainage system. However, combined with the previous two sections, it can be seen that the pressure extremes when discharging fecal sludge created more minor changes compared to the enteric-coated solids.

4.4. Mechanism analysis

The mechanism of the air pressure regime in the building drainage system is shown in Figure 15. The air pressure fluctuation of discharge solids was more significant than only discharge freshwater. According to the previous analysis, it is noticed that the trend of air pressure fluctuation in the drainage system is the same as that of the freshwater, and the total pressure loss in the stack is:

$$\Delta P_{\text{total}} = \Delta P_1 + \Delta P_2 + \Delta P_3 + \Delta P_4 \tag{9}$$

where ΔP_1 is the pressure loss at the inlet of the vent cap, Pa; ΔP_2 is the linear pressure loss in the dry pipe, Pa; ΔP_3 is the pressure loss caused by the discharging water and solids, Pa; and ΔP_4 is the pressure loss caused by the hydraulic jump, Pa.
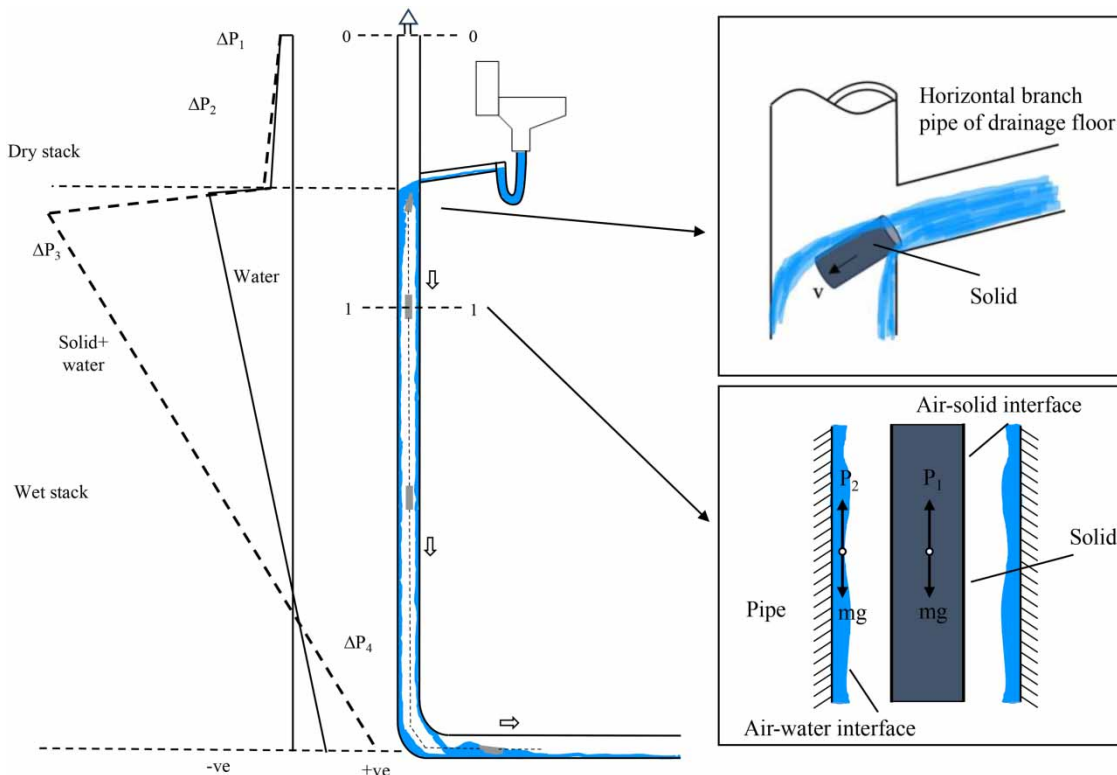

Figure 15 | Pressure regime within a building drainage system.

With the addition of the solids, the water flow and the solids together reached a steady state, as shown in Figure 15, for sections 0-0 and 1-1:

$$\frac{v_0^2}{2g} + \frac{P_0}{\rho g} = \frac{P_1}{\rho g} + \left(1 + \xi + \sum h_f + \varepsilon K_{inlet}\right)\frac{v_1^2}{2g} \tag{10}$$

where v_0 is the air flow rate at section 0-0, m/s; g is gravitational acceleration, m/s^2; ρ is density, kg/m^3; P_0 is the pressure at section 0-0, Pa; K_{inlet} is the local resistance coefficient caused by the water curtain at the branch-to-stack junction; ε is the coefficient of the solid's influence on the water curtain; ξ is the local resistance coefficient at the air inlet at the top of the pipe, which is generally taken to be 0.5; h_f is the linear loss, Pa; P_1 is the pressure at section 1-1, which is the negative pressure extreme value, Pa; v_1 is the terminal flow velocity, m/s.

With $v_0 = 0$ and $P_0 = 0$, simplify Equation (10) to:

$$P_1 = -\rho\left(1.5 + \sum h_f + \varepsilon K_{inlet}\right)\frac{v_1^2}{2} \tag{11}$$

When the system drained water only, the negative pressure was proportional to the terminal flow rate. When adding solids to the stack, the terminal flow velocity v_1 had an optimistic correlation with the solid velocity since the air in the stack was subjected to the shear forces of the solids and the water film. The solids increased the drag coefficient K_{inlet} at the water tongue, and its influence coefficient was denoted by ε. Similarly, the addition of solids affected the air–solid interface and the air–liquid interface in the vertical stack, which increased the frictional resistance coefficient h_f. That was the mechanism by which solids affect negative pressure in drainage systems.

From the previous analysis, the more significant the mass factor of solids, the greater the terminal flow velocity v_1 increased, which affected the air flow rate of the stack. Because of that, the negative pressure extreme value increased.

However, when the pipe diameter was reduced to De90, the solids in the stack lowered the air channel, causing the three-phase flow process to become more turbulent. Therefore, the shear force of the interface between air, water, and solid was increased, which caused an increase in the resistance coefficient h_f. The cross-section factor was more suitable to characterize the negative pressure extreme value variation at this time.

In the context of fecal sludge discharge, the rise in viscosity introduced a coefficient of influence, denoted as ε, affecting the local loss, K_{inlet}, at the water curtain. Simultaneously, in the vertical stack, the shear force between air and fecal sludge, influenced by viscosity, increased the falling process resistance, denoted as hf. Consequently, the negative pressure extremes were inclined to escalate. However, it is noteworthy that, on a holistic scale, the magnitude of this change remains relatively modest.

In the drainage system, the positive pressure extremes manifested at the bottom of the vertical pipe. The inflowing water into the horizontal drain pipe underwent distinct phases, including a rapid section, hydraulic jump, hydraulic jump completion, and gradual attenuation. According to the energy conservation equation, the hydraulic jump was analyzed before and after:

$$Z_1 + h_1 + \frac{v_1^2}{2g} = Z_2 + h_2 + \frac{v_2^2}{2g} + \Delta H \tag{12}$$

where Z_1, Z_2 is the position head before and after the jump, m; h_1, h_2 is the pressure head before and after the jump, m; v_1, v_2 is the flow velocity before and after the jump, m/s; ΔH is the head loss between the section of hydraulic jump, which mainly comes from the local head loss produced by the hydraulic jump and the friction head loss, m.

Since the pipe slope is constant, Equation (12) can be simplified as:

$$\Delta H = \left(\frac{v_1^2}{2g} - \frac{v_2^2}{2g}\right) + H_j \tag{13}$$

When discharged, solids possessed considerable kinetic energy during the drop in the vertical stack, which caused a more evident hydraulic jump in the horizontal drain pipe. Previous analyses indicated that as the mass factor increased, the height

difference of the hydraulic jump H_j and the velocity of the water v_1 increased, leading to an increase in ΔH. Consequently, the extreme value of the positive pressure within the drainage system was directly correlated to the mass factor. Additionally, as observed in prior analyses, the height difference H_j increased with the cross-section factor. Although this trend may not be as conspicuous as the mass factor, the extremum of positive pressure also escalated with the growing cross-section factor.

During the discharging of fecal sludge, H_j was more significant as the viscosity increased. The flow velocity gradient $(v_1^2 - v_2^2)/2g$ rose similarly. Consequently, the positive pressure extremes increased.

Therefore, when discharging enteric-coated solid, it is found that the pressure extremes are more drastic than fecal sludge. The mass factor and the cross-section factor have a more significant impact on the positive pressure of the system. In contrast, the viscosity of fecal sludge has a slightly higher effect on the positive pressure fluctuation of the drainage system.

5. CONCLUSIONS

By building a single-stack drainage system and CFD simulation, the effect of solids on the pressure fluctuation of a drainage system was investigated. The main conclusions are as follows:

(1) The positive and negative pressure extremes, air flow rate, and hydraulic jump fullness of the system are positively correlated with mass, cross-section, and viscosity factors. As the mass factor increased, the growth rates of positive and negative pressure extremes of the system under De110 and De90 pipe diameters were 2.30, 7.72% and 1.94, 4.34%, respectively. With the increase of cross-section factor, the system's positive pressure extremes growth rate was 2.69–2.88%, and negative pressure was 11.92–16.52%. For viscosity, the growth rate of positive pressure extremes of the system was 2.71–3.41%, and negative pressure was 0.56–1.46%.
(2) With the addition of solids, the terminal flow rate of airflow is increased by the solids. The solids increased the drag coefficient caused by the water curtain in the branch to the junction and the interaction forces between the three-phase flow in the vertical stack, resulting in a more significant pressure drop in the drainage system.
(3) Hydraulic jump fullness is the main reason for the variation of positive pressure extremes in the drainage system. With a growing mass factor and cross-section factor, the terminal flow rate and the height difference between the hydraulic jump increased, which resulted in more significant energy loss.

This research aims to explore the effect of solids on pressure fluctuations in a four-story single-stack drainage system from three perspectives. Due to the limited time, only enteric-coated solids and fecal sludge simulant were used in the experiment. Future studies would further propose different types of solid simulants that can be supplemented of this research. In addition, with the popularization of high-rise buildings, the building drainage system is becoming more complex, so it is necessary to explore the type and height of the building drainage system that may influence the pressure fluctuation.

ACKNOWLEDGEMENTS

DATA AVAILABILITY STATEMENT

All relevant data are included in the paper or its Supplementary Information.

CONFLICT OF INTEREST

The authors declare there is no conflict.

REFERENCES

Akhiyarov, D. T., Zhang, H.-Q. & Sarica, C. 2010 High-viscosity oil-gas flow in vertical pipe. In: *Offshore Technology Conference*. OTC, OTC-20617-MS.
Arnell, N. W., Van Vuuren, D. P. & Isaac, M. 2011 The implications of climate policy for the impacts of climate change on global water resources. *Global Environmental Change* **21**, 592–603.

Baroni, B., Oliveira, L., Comas, F. & Ota, I. 2018 Drain diameter reduction in a two-storey residential building drainage system for optimised performance to water conservation. In: *Proceedings of 44th International Symposium CIB W062 on Water Supply and Drainage for Buildings*, Ponta Delgada, Azores, Portugal, pp. 28–30.

Bhagat, R. K., Jha, N., Linden, P. & Wilson, D. I. 2018 On the origin of the circular hydraulic jump in a thin liquid film. *Journal of Fluid Mechanics* **851**, R5.

Campbell, D. 2017 Empirical derivation of flow parameters describing the behaviour of a novel artificial test solid for building drainage systems. *Building Services Engineering Research and Technology* **39**, 38–49.

Cheng, C., Yen, C., Wong, L. T. & Ho, K. 2008 An evaluation tool of infection risk analysis for drainage systems in high-rise residential buildings. *Building Services Engineering Research and Technology* **29**, 233–248.

Demarco, P., Koeller, J., Martin, S., Swatkowski, L. & Burgess, M. 2013 The drainline transport of solid waste in buildings. In: *Proceedings of CIB-W062 Symposium*, pp. 93–104.

Dolnicar, S., Hurlimann, A. & Grün, B. 2012 Water conservation behavior in Australia. *Journal of Environmental Management* **105**, 44–52.

Du, M., Liao, L., Wang, B. & Chen, Z. 2021 Evaluating the effectiveness of the water-saving society construction in China: A quasi-natural experiment. *Journal of Environmental Management* **277**, 111394.

Foster, S. & Ait-Kadi, M. 2012 Integrated water resources management (IWRM): How does groundwater fit in? *Hydrogeology Journal* **20**, 415–418.

Friedler, E., Katz, I. & Dosoretz, C. G. 2008 Chlorination and coagulation as pretreatments for greywater desalination. *Desalination* **222**, 38–49.

Gao, H., Wei, T., Lou, I., Yang, Z., Shen, Z. & Li, Y. 2014 Water saving effect on integrated water resource management. *Resources, Conservation and Recycling* **93**, 50–58.

General Administration Of Quality Supervision. 2015 I. A. Q. O. T. P. S. R. O. C. S. A. O. T. P. S. R. O. C. Sanitary wares.

Gormley, M. 2007 Air pressure transient generation as a result of falling solids in building drainage stacks: Definition, mechanisms and modelling. *Building Services Engineering Research and Technology* **28**, 55–70.

Gormley, M., Kelly, D., Campbell, D., Xue, Y. & Stewart, C. 2021 Building drainage system design for tall buildings: Current limitations and public health implications. *Buildings* **11**, 70.

Guan, Y. 2022 *Study on Discharge Capacity Under the Influence of Ventilation and Installation Modes on Double Stack Drainage System in High-Rise Residential Buildings*. Doctor's Degree Thesis, Wuhan University, Wuhan, China.

Guan, Y., Fang, Z., Tang, Z. & Yuan, J. 2020 Influence of the vent pipe diameter on the discharge capacity of a circuit vent building drainage system. *Building Services Engineering Research and Technology* **41**, 5–24.

Guo, Y., Yan, X., Shang, Y., Guan, Y. & Fang, Z. 2023 Influence of offset terminal elbow shape on the discharge capacity of a high-rise building drainage system. *Journal of Pipeline Systems Engineering and Practice* **14**, 04023028.

Lewis, S. J. & Heaton, K. W. 1997 Stool form scale as a useful guide to intestinal transit time. *Scandinavian Journal of Gastroenterology* **32**, 920–924.

Li, B., Guo, Z., Chen, R. & Zhang, B. 2015 Experimental study on sediment deposition and water level surge under strong sediment transport in variable slope gradient channel. *Journal of Sediment Research* **3**,63–68.

Lillywhite, M., Wise, A. F. E. & Wise, A. 1969 *Towards a General Method for the Design of Drainage Systems in Large Buildings*. Building Research Station, London, UK.

McDougall, J. A. & Swaffield, J. 2000 Simulation of building drainage system operation under water conservation design criteria. *Building Services Engineering Research and Technology* **21**, 41–51.

McDougall, J. & Swaffield, J. 2003 The influence of water conservation on drain sizing for building drainage systems. *Building Services Engineering Research and Technology* **24**, 229–243.

Miranda, J. D. D., Armas, C., Padilla, F. & Pugnaire, F. 2011 Climatic change and rainfall patterns: effects on semi-arid plant communities of the Iberian Southeast. *Journal of Arid Environments* **75**, 1302–1309.

Mupinga, R. T., Septien, S., Pocock, J. & Buckley, C. 2020 An investigation into the stickiness of faecal sludge: Preliminary investigation of VIP and UDDT sludge with varying moisture content at ambient temperature. *Gates Open Research* **4**, 78–90.

Najafzadeh, M. 2019 Evaluation of conjugate depths of hydraulic jump in circular pipes using evolutionary computing. *Soft Computing*.

Penn, R., Ward, B. J., Strande, L. & Maurer, M. 2018 Review of synthetic human faeces and faecal sludge for sanitation and wastewater research. *Water Research* **132**, 222–240.

Radford, J., Underdown, C., Velkushanova, K., Byrne, A., Smith, D., Fenner, R., Pietrovito, J. & Whitesell, A. 2015 Faecal sludge simulants to aid the development of desludging technologies. *Journal of Water, Sanitation and Hygiene for Development* **5**, 456–464.

Swaffield, J. & Campbell, D. 1995 The simulation of air pressure propagation in building drainage and vent systems. *Building and Environment* **30**, 115–127.

Swaffield, J., Jack, L. & Campbell, D. 2004 Control and suppression of air pressure transients in building drainage and vent systems. *Building and Environment* **39**, 783–794.

Tanabe, Y., Sakaue, K., Ogami, M. & Okauchi, S. Experimental studies on the influence that excessive waste and form of fixture discharge pipes exert on seal water *CIB W062 Conference* **1**, 155–166.

Wang, Z., Zhang, X. & Chen, J. 1992 Experimental study on hydraulic characteristics of slurry. *Journal of Sediment Research* **3**, 1–12.

Wise, A. F. E. & Swaffield, J. A. 2012 *Water, Sanitary and Waste Services for Buildings*. Routledge, Abingdon, Oxfordshire, UK.

Wyly, R. S. 1952 *Capacities of Plumbing Stacks in Buildings*. US Department of Commerce, National Bureau of Standards, Washington, DC, USA.

Wyly, R. S. & Eaton, H. N. 1961 *Capacities of Stacks in Sanitary Drainage Systems for Buildings*. US Department of Commerce, National Bureau of Standards, Washington, DC, USA.

Wyly, R., Benazzi, R., Konen, T., Manfredi, R., Nielsen, L., Maybeck, E. & Schnarr, R. 1979 Hydraulics of gravity drainage systems. In: *Water Supply and Drainage in Buildings: Proceedings of an International Symposium*, September 28–30, 1976. National Academy of Sciences, Washington, DC, USA, 35.

Xu, P., Fu, B. & Song, Y. 2023 Experimental study on the hydraulic performance of the horizontal main drain of building drainage systems with solid waste. *Journal of Hydroinformatics* **25**, 1844–1860.

Zhang, Y. 2018 *Study of Drainage Characteristics and Optimization of Special Single Stack System in Super High-Rise Buildings*. MA dissertation. Wuhan University of Technology, Wuhan, China.

Zhang, Z. 2022 The determination and establishment of the undetermined coefficient value of the final limit formula of the smooth zone of the drainage riser, the final limit formula of the transition zone and the thickness formula of the viscous bottom layer. In: *The 4th First All-Member Conference and Academic Exchange Meeting of Building Water Supply and Drainage Research Branch of Chinese Architectural Society, Xiamen*, Fujian, China.

Zhang, M., Shrestha, P., Liu, X., Turnaoglu, T., Degraw, J., Schafer, D. & Love, N. 2022 Computational fluid dynamics simulation of SARS-CoV-2 aerosol dispersion inside a grocery store. *Building and Environment* **209**, 108652.